Ultralong-Life Quasi-Solid-State Li-O$_2$ Batteries Enabled by Coupling Advanced Air Electrode Design with Li Metal Anode Protection

Changtai Zhao, Jianneng Liang, Qian Sun, Jing Luo, Yulong Liu, Xiaoting Lin, Yang Zhao, Hossein Yadegari, Mohammad Norouzi Banis, Ruying Li, Huan Huang, Li Zhang, Rong Yang, Shigang Lu, and Xueliang Sun*

Development of Li-O$_2$ batteries with ultrahigh theoretical energy density is highly desired to meet the ever-increasing demand of energy density. However, safety concerns and cycling life have become main bottlenecks that inhibit the practical applications of Li-O$_2$ batteries because of the use of organic liquid electrolytes (LEs) and the noneffective air electrodes. Gel polymer electrolytes (GPEs) are reported to be used in Li-O$_2$ batteries and show relatively improved performance than LEs, but they are still below the expectation. Herein, a quasi-solid-state Li-O$_2$ battery constructed with a GPE and a high-efficiency air electrode is proposed. Excellent electrochemical performance is demonstrated beyond the batteries with LE, evidenced by the ultralong cycle life of up to 553 cycles and stable operating time for over 1100 h. The elongated cycling life benefits from the role of GPE in blocking O$_2$ crossover, protecting Li metal, and avoiding electrolyte evaporation compared with LE. It is expected that the present study can shed light on the future study on developing efficient catalysts for (quasi) solid-state Li-O$_2$ battery.

1. Introduction

The ever-growing demands of electrochemical energy storage systems with higher energy density have stimulated worldwide research interests toward development of Li-O$_2$ batteries owing to the ultrahigh theoretical energy density up to 3500 W h kg^{-1}.[1] However, the use of conventional organic liquid electrolytes (LEs) has brought safety hazards associated with the leakage and flammability of organic LEs, especially in Li-O$_2$ batteries with an open system.[2] Another intrinsic drawback of using LEs in Li-O$_2$ batteries is the undesired and inevitable formation of Li dendrites, which is mainly triggered by the inhomogeneous Li ions distribution on the surface of Li metal due to the high electric field near tips (commonly known as "tip effect").[3] This is a common problem in Li metal batteries. Whether the problem can be resolved properly directly determines the practicality of Li metal. Moreover, the evaporation of LEs and their failure in inhibiting O$_2$ crossover are also serious concerns that hamper the development of Li-O$_2$ batteries.[4] In this context, replacing organic LEs with (quasi) solid-state electrolytes (SSEs) is a strategy to overcome these shortcomings and achieve high safety.[5] Among the possible candidates, ceramic SSEs are shown to suppress Li dendrite growth, but most of reported ceramic SSEs feature relatively low ionic conductivity and high interfacial resistance with electrodes, in turn leading to deterioration of electrochemical performance. In particular, the drawbacks would be exacerbated in Li-O$_2$ batteries which intrinsically feature sluggish electrochemical dynamics.[6] Meanwhile, most ceramic SSEs are chemically unstable against Li metal.[7] Alternatively, polymer SSEs show additional advantages in scalability and processability, but they usually require operation at higher temperatures than room temperature, which will increase the difficulty and complexity of the operation condition and may trigger more side reactions in Li-O$_2$ batteries.[5c,d,7,8] For the development of safe solid-state Li-O$_2$ batteries, all these drawbacks need to be overcome.

Gel polymer electrolytes (GPEs), combing the high ionic conductivity of LE and the mechanical properties of polymer SSE, have drawn considerable attentions for being used as both electrolyte and separator.[9] Besides, GPEs can render the energy storage devices with adjustable shapes and high flexibility, which is promising for the burgeoning portable and wearable electronics. With these merits, GPEs have been reported to be used in Li-O$_2$ batteries and show relatively improved

Dr. C. Zhao, J. Liang, Dr. Q. Sun, J. Luo, Dr. Y. Liu, X. Lin, Y. Zhao,
Dr. H. Yadegari, Dr. M. N. Banis, R. Li, Prof. X. Sun
Department of Mechanical and Materials Engineering
University of Western Ontario
London, ON N6A 5B9, Canada
E-mail: xsun9@uwo.ca
Dr. H. Huang
Glabat Solid-State Battery Inc.
700 Collip Circle, London, ON N6G 4X8, Canada
Dr. L. Zhang, Dr. R. Yang, Dr. S. Lu
China Automotive Battery Research Institute
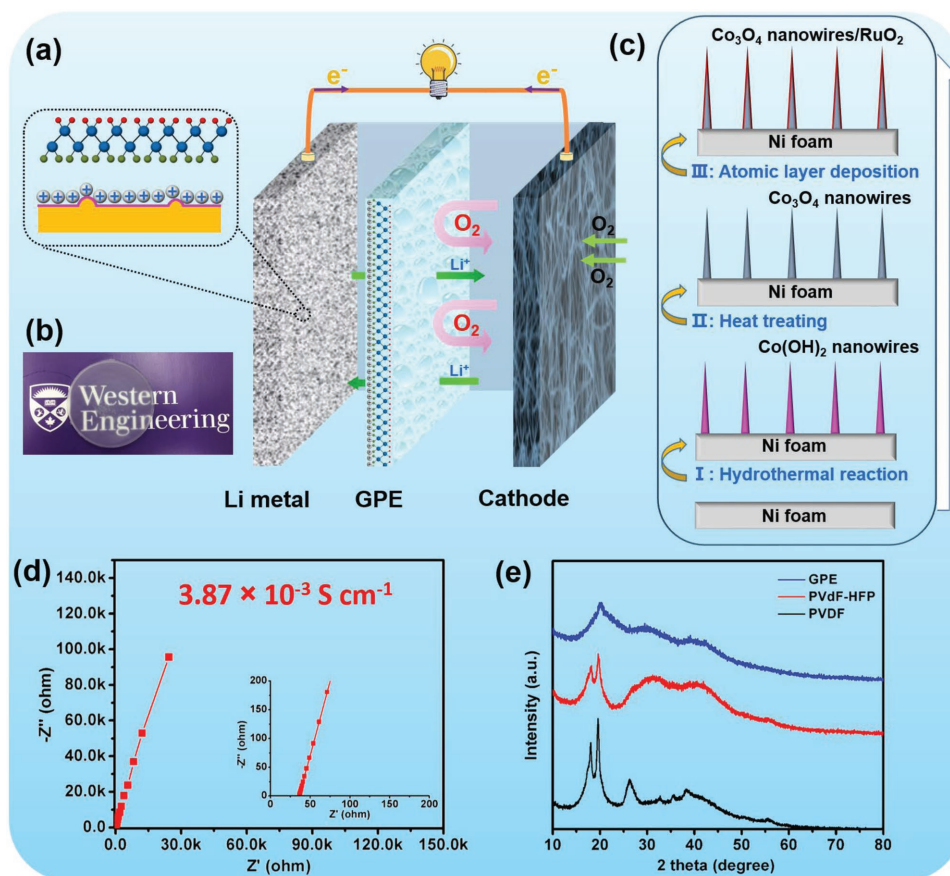Beijing 100088, P. R. China

Figure 1. a) Schematic illustration of a Li-O$_2$ battery with GPE. b) The digital photograph of the as-prepared GPE. c) Schematic for the synthesis process of Ni foam@Co$_3$O$_4$-50RuO$_2$. d) Nyquist plot of GPE for calculating the ionic conductivity, and the inset is a magnified Nyquist plot. e) XRD patterns of the PVDF, PVDF-HFP, and GPE.

performance than LEs, but still below the expectation.[10] Some previous references reported the use of some kinds of catalysts to prolong their life up to 200–400 cycles.[10c,11] Nonetheless, longer cycling life is still required for practical usage. So pairing efficient air electrode with advanced GPEs may be an effective strategy to achieve ultralong-life Li-O$_2$ batteries. Besides, to our best knowledge, there is no comprehensive study on GPE application in Li-O$_2$ batteries that simultaneously address the interfacial resistance with electrodes, Li deposition behavior, O$_2$ crossover, and electrolyte evaporation, while these concerns are extremely important for practical applications and research of GPEs.

Herein, we demonstrate a quasi-solid-state Li-O$_2$ battery pairing a GPE with a high-efficiency air electrode to realize long-term cycling life. The comprehensive properties of GPE, including ionic conductivity, interfacial compatibility, Li deposition behavior, O$_2$ crossover, and electrolyte evaporation, were investigated in detail and compared with LE. The highly ionic conductive GPE showed low interfacial resistance with electrodes, being comparable to LE. The GPE containing a polar β-phase poly(vinylidene fluoride-co-hexafluoropropylene) (PVDF-HFP) also featured regulation on Li deposition behaviors. The polar functional groups in the GPE enabled uniform distribution of Li ions in the GPE and at the interface with Li metal and thus led to dendrite-free Li metal deposition.

Meanwhile, the GPE prevented O$_2$ crossover and electrolyte evaporation. Because of the merits of the GPE and the high catalytic activity of the air electrode, the proposed Li-O$_2$ battery exhibited ultralong cycle life up to 553 cycles and operation time over 1100 h.

2. Results and Discussion

Figure 1a is the schematic illustration of a Li-O$_2$ battery with GPE. It shows the components of battery and the contribution of using GPE on the regulation of Li metal deposition and the prevention of O$_2$ crossover. The GPE was made of PVDF-HFP polymer, tetraethylene glycol dimethyl ether (TEGDME) solvent, and LiClO$_4$ salt. As shown in Figure 1b, the as-made GPE is a free-standing and translucent film, which can be used as both the electrolyte and separator in Li-O$_2$ battery.[12] The ionic conductivity of GPE was evaluated by electrochemical impedance spectroscopy (EIS) (Figure 1d) and determined to be $\approx 3.87 \times 10^{-3}$ S cm^{-1}, comparable to that of LE in glass fibers separator ($\approx 10.40 \times 10^{-3}$ S cm^{-1}). The composition and crystalline structure of the as-prepared GPE were also investigated by X-ray diffraction (XRD). As shown in Figure 1e, both PVDF and PVDF-HFP dry powders showed a dominant crystalline structure of α-phase PVDF by the characteristic peaks at 17.7°, 18.3°,

**ADVANCED
SCIENCE NEWS**
www.advancedsciencenews.com
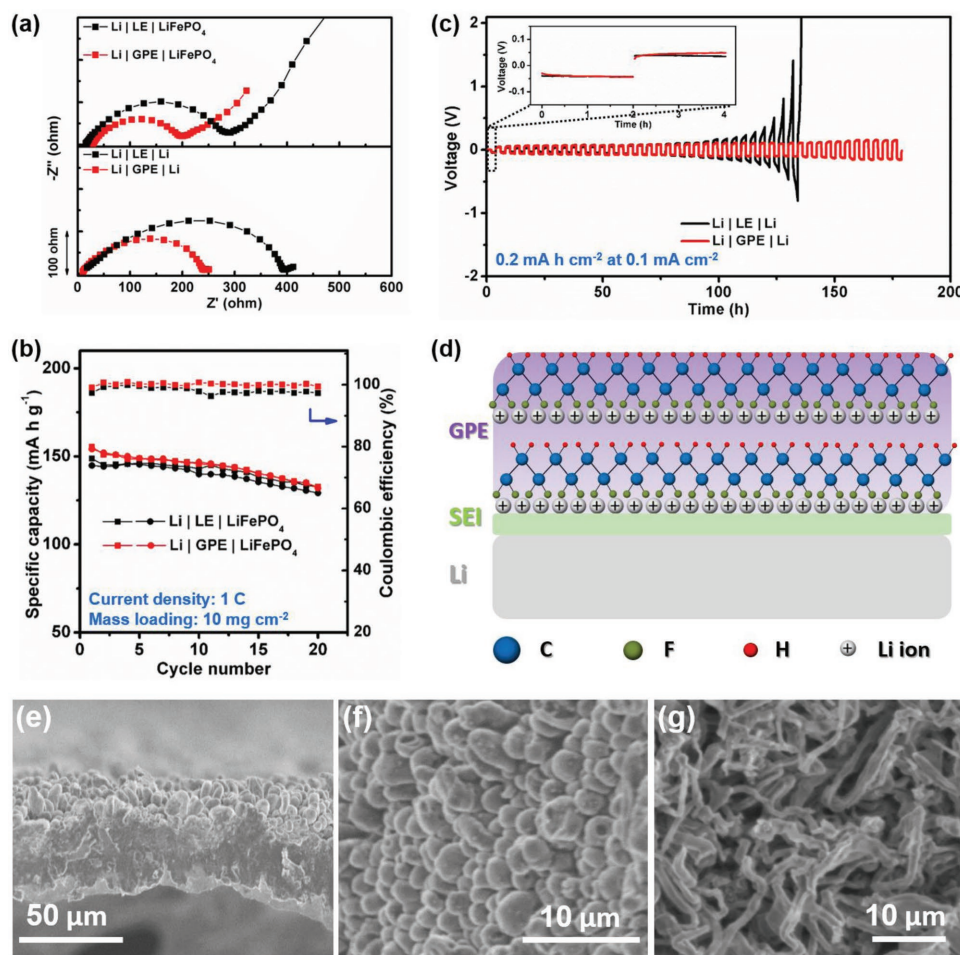
**small
methods**
www.small-methods.com

Figure 2. a) Nyquist plots of LiFePO₄ full cells and Li metal symmetric cells with LE and GPE. b) The cycling performance of LiFePO₄ full cells with LE and GPE. c) The cycling performance of Li metal symmetric cells with LE and GPE, and the inset shows the corresponding 1st cycle discharge/charge curves. d) Schematic illustration of Li deposition behavior with GPE. SEM images of Cu foils after plating 2 mA h cm⁻² of Li at 0.5 mA cm⁻² in the e,f) GPE and g) LE based cells.

and 19.9°, while the β phase (20.3°) became dominant as the PVDF-HFP processed into GPE. Detailed explanations will be presented in later discussion.

In addition to the high ionic conductivity of the bulk GPE, the interfacial resistances of GPE toward Li metal anode and LiFePO₄ cathode were further investigated. Full cells with a LiFeO₄ cathode and a Li metal anode as well as symmetric cells with two Li metal electrodes were assembled for EIS evaluations. Two different electrolytes, GPE and LE, were compared. The same LiClO₄ salt and TEGDME solvent were used in both GPE and LE, but LE required an additional separator, a polypropylene Celgard 2400 in this case. As shown in **Figure 2**a, the cells using GPE showed similar and even smaller charge transfer resistances (R_{CT}) compared to the cells using LE, no matter in full-cell or symmetric-cell configuration. In other words, the interfacial resistances between electrodes and electrolytes were similar, and even smaller with GPE than with LE. This also suggested good compatibilities between GPE and Li metal anode or LiFePO₄ cathode. These results can also be proved by the cycling performance of LiFePO₄ full cells at 1 C (Figure 2b). It is worth noting that the cell using GPE showed

higher specific capacity and better Coulombic efficiency than those of the cell using LE.

The Li metal cycling stability using GPE was studied in a Li metal symmetric cell configuration. Figure 2c compares the cycling performance of the cells with GPE or LE at a current density of 0.1 mA cm⁻² and a capacity of 0.2 mA h cm⁻². The two cells showed similarly low overpotential at the 1st cycle, again confirming the high ionic conductivity and low interfacial resistance of the GPE as LE. However, the cycling stabilities were different. The LE cell encountered a rapid increase in overpotential after 100 h of cycling, while the cell using GPE remained highly stable even up to 170 h. The GPE was demonstrated to facilitate a more favorable Li deposition behavior than a typical LE. Since the same salt and solvent were used in GPE and LE, PVDF-HFP, as the polymer matrix of the GPE instead of a polypropylene separator for LE, evidently played an important role in regulating the Li metal deposition.[10d]

The superior cycling stability with GPE could be attributed to the unique properties of the PVDF-HFP component. As mentioned in XRD part above, the originally nonpolar α-phase PVDF-HFP was readily transformed into an exclusive
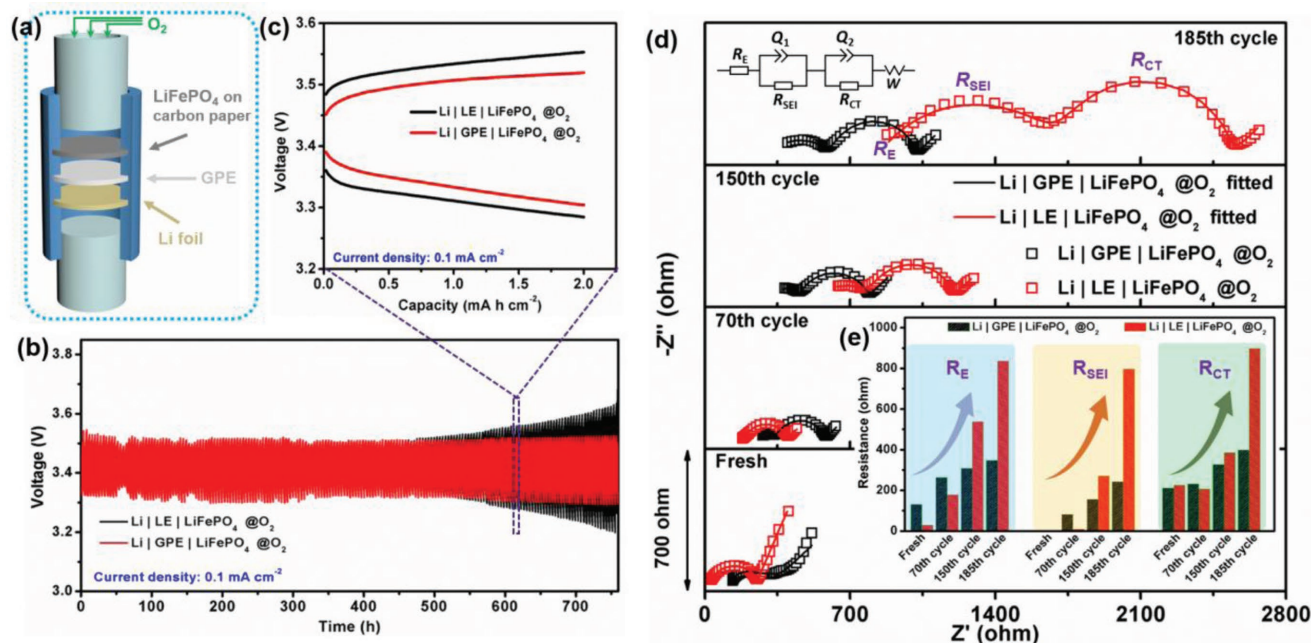
Figure 3. a) Schematic illustration of the LiFePO$_4$ full cell with GPE in O$_2$ atmosphere. b) The cycling performance of LiFePO$_4$ full cells using LE and GPE with a limited capacity of 0.2 mA h cm^{-2} at the current density 0.1 mA cm^{-2} in O$_2$ atmosphere. c) The 150th cycle discharge/charge profiles of LiFePO$_4$ full cells with LE and GPE. d) Nyquist plots of LiFePO$_4$ full cells with LE and GPE in O$_2$ atmosphere at different cycles, the inset is the equivalent circuits for fitting the Nyquist plots. e) The histograms of the fitted R_E, R_{SEI}, and R_{CT} values of LiFePO$_4$ full cells with LE and GPE in O$_2$ atmosphere after different cycles.

polar β phase when processed into GPE. Presumably, interactions between the polar aprotic solvent, TEGDME, and the PVDF-HFP had induced rearrangement of polymer chains. Particularly, PVDF possesses different crystalline phases, corresponding to different F and H atom alignments along the polymer backbone comprising of [CH$_2$CF$_2$] motifs.[13] Among them, β phase features the most polar form, in which all F and H atoms are located on the opposite sides of the polymer backbone as *trans* conformation, resulting in a high dielectric constant (8–13);[14] on the other hand, α phase features a *trans*-gauche-*trans*-gauche conformation so that the dipole moments are offset within the unit cells. In the case of GPE, these polar functional groups (C−F) with ordered alignment on the polymer backbone can regulate Li ions via strong chemical affinity with Li ions, leading to the uniform distribution of Li ions in the GPE and at the interface with Li metal (Figure 2d).[15] As a result, the Li dendrite formation, rooted mainly from the inhomogeneous Li-ion distribution on the Li metal surface due to "tip effects," can be largely mitigated.[16] Specifically, "tip effects" refer to the large local electric field intensity at surface protrusions that attract Li ions and promote nucleation and growth of Li dendrites.[17] If tips are inevitable, an effective strategy to realize uniform Li-ion distribution is crucial.[18] In our GPE, Li ions were believed to be redistributed due to the strong affinity between the β-phase PVDF-HFP and Li ions. As a result, the tip effects can be mitigated to a certain extent, and thus suppressing Li dendrite formation and reducing accumulation of "dead Li." [15–18] Eventually, the symmetric cell with GPE showed a lower polarization than that with LE.

The regulation of Li metal deposition behavior by the GPE can also be evidenced by scanning electron microscopy (SEM) analysis. Using GPE or LE independently, 2 mA h cm^{-2} of Li was plated onto a Cu foil substrate at a current density of 0.5 mA cm^{-2} for morphological examination. As shown in Figure 2e,f and Figure S1 (Supporting Information) for the cell with GPE, the deposited Li metal featured column-like morphology rather than dendritic Li.[3b,19] In sharp contrast, the deposited Li metal with LE showed typical Li dendrite characteristics (Figure 2g).

In addition to regulating Li deposition, protecting the Li metal anode from O$_2$ is another equally important task for Li-O$_2$ batteries. Here, a special cell configuration was designed to study the O$_2$ crossover behaviors in the system and to gain insights into the effects of GPE on preventing O$_2$ crossover. As schematically shown in **Figure 3**a, a typical cell contains Li metal as the anode, GPE as the electrolyte and separator, and LiFePO$_4$ loaded porous carbon paper as the cathode, where the cathode side is open to an O$_2$ atmosphere. For a control cell, the GPE was replaced by LE and a separator. Before the cycling test, the cells were charged to 4.2 V. The cycling performance test was performed at a current density of 0.1 mA cm^{-2} with a limited capacity of 0.2 mA h cm^{-2} (Figure 3b,c). Unlike the cell using LE that gradually increased in overpotential after 500 h, the cell with GPE was highly stable for more than 750 h. Evidently, the GPE was playing a positive role in protecting Li metal and electrolyte against the O$_2$ atmosphere.

Meanwhile, real-time EIS evolution was measured to further understand the long-term stability and effectiveness in preventing O$_2$ crossover. Figure 3d shows the EIS spectra and the
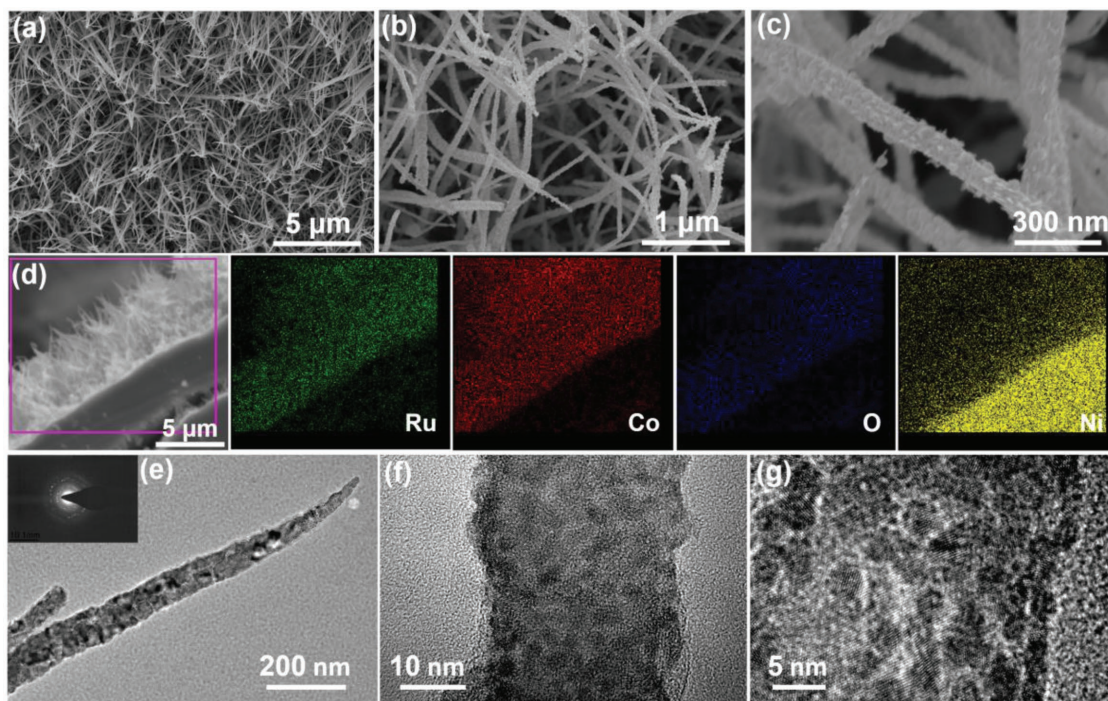
**ADVANCED
SCIENCE NEWS**

www.advancedsciencenews.com

**small
methods**

www.small-methods.com

Figure 4. a–c) SEM images of the as-prepared Ni foam@Co$_3$O$_4$. d) SEM image of Ni foam@Co$_3$O$_4$-50RuO$_2$ and the corresponding elemental mapping images of Ru, Co, O, and Ni. e) TEM and f,g) HRTEM images of Ni foam@Co$_3$O$_4$-50RuO$_2$, the inset in (e) is the corresponding selected-area electron diffraction pattern.

corresponding fitted curves based on the equivalent circuits, and Figure 3e summarizes the fitted results, including the electrolyte resistance (R_E), the interface resistance (R_{SEI}), and the charge-transfer resistance (R_{CT}). The fresh cells with either GPE or LE show similar R_{CT} values initially. However, with increasing cycle number, all the resistance values (including R_E, R_{SEI}, and R_{CT}) of the LE cell increased much more dramatically than the GPE cell, especially after 150 cycles (i.e., 600 h of cycling) coinciding with the trend of overpotentials (Figure 3c). For instance, after 185th cycle (i.e., 740 h of cycling), the R_E, R_{SEI}, and R_{CT} of the cell with LE were 837, 796, and 899 Ω, respectively, which were significantly larger than those of the cell with GPE (R_E = 348 Ω, R_{SEI} = 242 Ω, and R_{CT} = 399 Ω). Compared with the relatively stable R_E values of the GPE cell, the booming R_E values of the LE cell could be attributed to the evaporation of LE in the open system during a long-time cycling process.[20] This is also a common and crucial problem of using LE in Li-O$_2$ batteries. Moreover, the cell with LE presented the markedly increased R_{SEI}, which suggested a severe corrosion occurring at the Li metal anode caused by the O$_2$ crossover.[21] The relatively stable R_{SEI} values of the GPE cell indicated an effective reduction in O$_2$ crossover by GPE and thus suppression on side reactions between the Li metal and O$_2$. In addition, another experiment was designed to verify the effect of GPE on blocking O$_2$ crossover (Figure S2 (Supporting Information)). Before assembling the symmetric cells, two kinds of Li foils were prepared by immersing it in LE and sealing it in GPE, respectively, for 24 h in O$_2$ atmosphere. As shown in the digital photos (Figure S2 (Supporting Information)), the Li foil sealed in GPE keeps originally metallic color. By contrast, the

color of the Li foil immersed in LE becomes dark, indicating the oxidation of Li metal. When the Li foils were assembled to Li metal symmetric cells, the cell with the Li foils immersed in LE showed a significantly increased resistance, suggesting an obvious surface corrosion. This test highlights again the GPE for blocking O$_2$ crossover. All in all, considering the high ionic conductivity, low interfacial resistance with both Li metal anode and cathode, regulation on Li metal deposition, mitigation of O$_2$ crossover, and alleviation of electrolyte evaporation, the proposed GPE can be a promising electrolyte for Li-O$_2$ batteries.

The electrochemical properties of the GPE in Li-O$_2$ batteries were evaluated with an effective air electrode, a composite of Co$_3$O$_4$ nanowires grown on Ni foam (Ni foam@Co$_3$O$_4$). The Ni foam@Co$_3$O$_4$ composite is free-standing. Thus, the composite can be used as the air electrode without any auxiliary binder, conductive agent, and current collector. In addition, this composite is carbon-free. This will avoid the side reactions associated with carbon during cycling process. As shown in **Figure 4**a–c, the Co$_3$O$_4$ nanowires ≈100 nm in diameter were vertically distributed on the surface of Ni foam. The Co$_3$O$_4$ nanowires construct the porous channels for O$_2$ diffusion and the storage of discharge products and also feature a high catalytic ability for decomposing the discharge products. To further optimize the electrochemical performance of Li-O$_2$ batteries, RuO$_2$ nanoparticles were uniformly deposited on Co$_3$O$_4$ nanowires (Ni foam@Co$_3$O$_4$-50RuO$_2$) by atomic layer deposition technique. The synthesis process is schematically illustrated in Figure 1c. As shown in Figure 4d, the resulting Ni foam@Co$_3$O$_4$-50RuO$_2$ maintained a basic morphology similar to the Ni foam@Co$_3$O$_4$, but the energy-dispersive X-ray spectroscopy
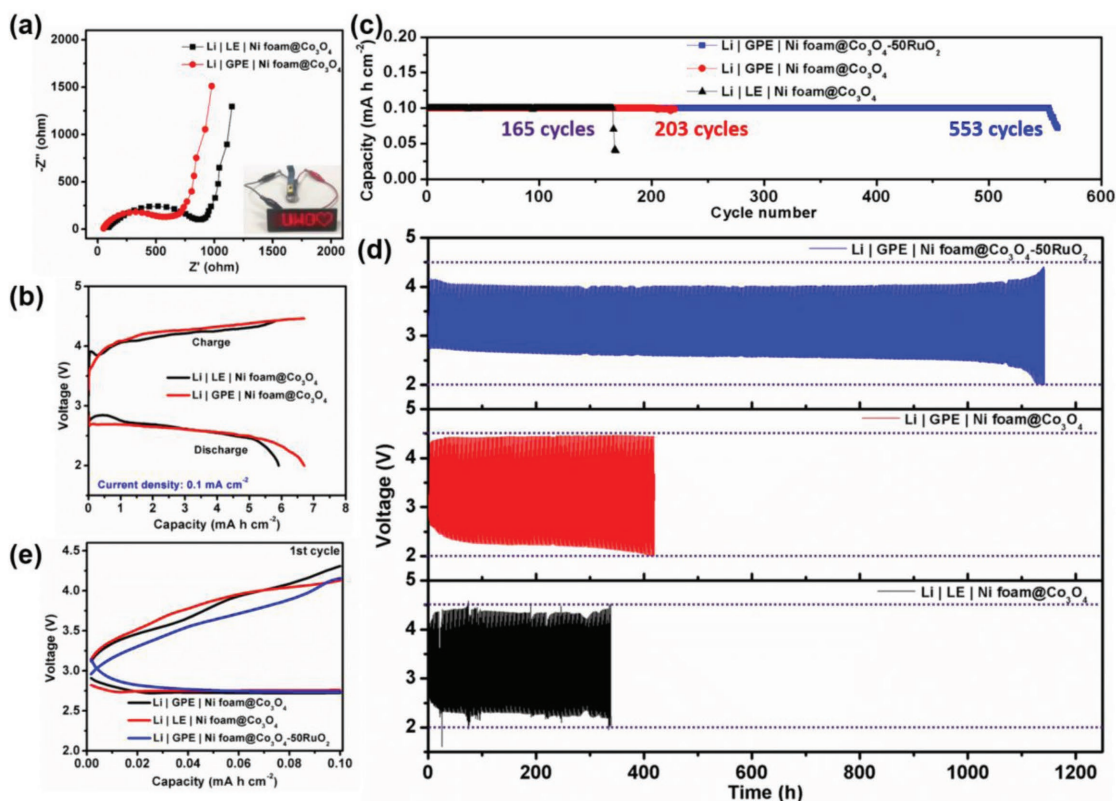
Figure 5. a) Nyquist plots of Li-O$_2$ batteries with LE and GPE, the inset is a digital photo of the LED screen powered by the coin cell built with GPE and Ni foam@Co$_3$O$_4$. b) Discharge/charge profiles of Li-O$_2$ batteries with LE and GPE at 0.1 mA cm^{-2}. c) Cycling performance of Li-O$_2$ batteries with LE and GPE at a current density of 0.1 mA cm^{-2}. d) Discharge/charge profiles of Li-O$_2$ batteries with LE and GPE at a current density of 0.1 mA cm^{-2}. e) The 1st cycle discharge/charge profiles of Li-O$_2$ batteries with LE and GPE.

(EDX) elemental mappings had confirmed the uniform distribution of RuO$_2$ on Co$_3$O$_4$ nanowires. The microscopic morphology and distribution of RuO$_2$ nanoparticles were further verified by transmission electron microscopy (TEM) and high-resolution TEM (HRTEM) analysis, indicating the uniform growth of RuO$_2$ nanoparticles with a particle size of ≈3 nm (Figure 4e–g). As a noble metal element, it is crucially important for reducing Ru dosage and fully fulfilling its efficacy.[20] The advantage of atomic layer deposition technique in depositing ultrafine nanoparticles on designated substrate with uniform distribution should be highlighted. The XRD patterns and X-ray photoelectron spectroscopy (XPS) spectra are provided in Figure S3 (Supporting Information), again confirming the presence of Co$_3$O$_4$ and RuO$_2$.

The electrochemical performance of Li-O$_2$ batteries with the as-prepared GPE and Ni foam@Co$_3$O$_4$ was evaluated by galvanostatic discharge/charge and EIS tests. Nyquist plots indicated a low initial R_{CT} of the cells, with an even smaller value of the GPE cell than that of the LE cell (**Figure 5**a). As shown in Figure 5b, the Li-O$_2$ battery with GPE delivered a high areal capacity of 6.7 mA h cm^{-2} which is even higher than the 5.9 mA h cm^{-2} of the LE cell. Upon subsequent charging, the GPE cell achieved to be fully recharged and exhibited similar operating voltage to the LE cell. Meanwhile, the battery could light the LED screen. The cycling performances of Li-O$_2$ batteries using either LE or GPE were compared by galvanostatic

discharge/charge tests. Upon cycling with a limited capacity of 0.1 mA h cm^{-2} at a current density of 0.1 mA cm^{-2}, the GPE cell was more stable and showed a longer cycle life than the LE cell (Figure 5c–d). The LE cell delivered an effective cycle life of 165 cycles with fluctuating polarizations, while the GPE cell maintained an enhanced cycle life of 203 cycles with stable operating voltages. The results were consistent with the beneficial effects of GPE in terms of Li anode protection and electrolyte conservation discussed previously.

The application of Ni foam@Co$_3$O$_4$-50RuO$_2$ air electrode in Li-O$_2$ battery with GPE further pushed the cycle life to ultralong 553 cycles and stable operation time for over 1100 h. By comparing the discharge-charge profiles of the different air electrodes (with or without RuO$_2$ nanoparticles) at the 1st cycle and 100th cycle, the presence of RuO$_2$ nanoparticles effectively decreased the overpotential and reduced polarizations upon the prolonged cycle life (Figure 5e and Figure S4 (Supporting Information)). Even with a large limited capacity of 0.3 mA h cm^{-2}, the Li-O$_2$ battery with a GPE and Ni foam@Co$_3$O$_4$-50RuO$_2$ air electrode achieved a cycle of 171 cycles and maintained stable overpotential for more than 1000 h (Figure S5 (Supporting Information)).

The morphologies of the Ni foam@Co$_3$O$_4$ after discharging and recharging in different electrolytes were investigated by SEM (Figure S6 (Supporting Information)). After discharging to 0.2 mA h cm^{-2}, the Ni foam@Co$_3$O$_4$ in both LE-based and GPE-based cells showed similar morphologies of nanosized

**ADVANCED
SCIENCE NEWS**

www.advancedsciencenews.com

**small
methods**

www.small-methods.com

discharge products deposited evenly and tightly on the surface of Co_3O_4 nanowires (Figure S6a,b (Supporting Information)). Interestingly, after fully recharging in the GPE-based cell, the discharge products almost disappeared with the Co_3O_4 skeleton well maintained (Figure S6c,d (Supporting Information)). This indicated a great catalytic activity of Ni foam@Co_3O_4 with GPE in the Li-O_2 battery. Meanwhile, the Co_3O_4 nanowires became porous and consisted of nanoparticles. The increased the active surface area may be in favor of enhancing the catalytic activity.

These encouraging results have indicated the versatile merits of the GPE as both electrolyte and separator in Li-O_2 batteries for high ionic conductivity, low interfacial resistances with both Li metal anode and cathode, regulation on Li metal deposition, reduction of O_2 crossover, and electrolyte conservation. To be honest, the mechanical strength of GPE alone is still not enough to completely prevent the penetration of Li dendrite for long-term cycling. Promising future directions include hybridizing GPE with mechanical strengthening skeletons or fillers, functionalizing the polymer matrix and other constituents, and utilization of appropriate additives in GPE to induce favorable solid electrolyte interphase (SEI) on Li metal anodes. These approaches are certainly of potential to design quasi/hybrid-solid state Li-O_2 batteries with high safety and high energy density.

3. Conclusion

In summary, we built a long-life Li-O_2 battery based on PVDF-HFP-based GPE and a high efficient air electrode. The proposed GPE features high ionic conductivity and low interfacial resistances toward both Li metal anode and cathodes (including common LiFePO$_4$ cathode and air electrodes). The superior performance of GPE is largely attributed to the unique phase transformation of PVDF-HFP during the fabrication process. A polar β-phase PVDF-HFP was formed, which is reported to have good chemical affinity with Li ions and could lead to uniform distribution of Li ions in the GPE and at the interface with Li metal. Hence, the common "tip effects" can be mitigated for better Li metal deposition and enhanced Li anode performance. In addition, the GPE was demonstrated to reduce O_2 crossover and electrolyte evaporation for open Li-O_2 systems. The ultralong cycling performance of 553 cycles and operation time for over 1100 h proved the viability of GPE in Li-O_2 batteries. We expect that the present study would provide motivations for developing (quasi) solid state Li-O_2 battery.

4. Experimental Section

Synthesis of the GPE: The GPE was prepared by a solution casting method. Typically, PVDF-HFP polymer was dissolved in acetone by vigorously stirring. Then, TEGDME and LiClO$_4$ were added into the above solution, and the solution was subjected to continuous stirring overnight. The resultant solution was casted in a polytetrafluoroethylene dish and dried at room temperature for two days to remove acetone solvent. The thickness of as-prepared GPE was about 1 mm.

Synthesis of the Ni Foam@Co_3O_4-50RuO$_2$: Ni foam was washed with 1 M HCl solution and alcohol to remove the oxide layer on the surface. Typically, 1.52 g of CoCl$_2$·6H$_2$O and 1.92 g of urea were dissolved into 80 mL of water under a continuous stirring. Then, the solution was transferred into 100 mL of Teflon-line stainless-steel autoclave and

a piece of pretreated Ni foam (4 cm × 5.5 cm) was infiltrated into the prepared solution. After holding at 95 °C for 8 h, Ni foam@Co(OH)$_2$ was yielded. The obtained Ni foam@Co(OH)$_2$ was annealed at 500 °C for 3 h in air with a ramping rate of 5 °C min^{-1}, yielding the product of Ni foam@Co_3O_4. The Ni foam@Co_3O_4-50RuO$_2$ was prepared by a typical atomic layer deposition process.

Materials Characterization: XRD (Bruker D8 Advance, Cu K α X-ray source), SEM (Hitachi S-4800), TEM (FEI TF30), and XPS (Thermo ESCALAB 250) were employed to examine the as-made GPE and Ni foam@Co_3O_4-50RuO$_2$.

Electrochemical Measurements: The Ni foam@Co_3O_4 and Ni foam@Co_3O_4-50RuO$_2$ were used as the cathode without any auxiliary binder, conductive agent or current collector. The areal mass of Co_3O_4 in this composite was about 1.52 mg cm^{-2}. The as-made GPE acted as both electrolyte and separator in quasi-solid-state cells. For comparison, the TEGDME solvent with 1 M LiClO$_4$ and polypropylene (Celgard 2400) were used as LE and separator, respectively, in liquid cells. The electrochemical performances of Li-O_2 batteries were evaluated by assembling Swagelok-type cells and testing on Arbin battery testing system in 1 atm O_2. The LiFePO$_4$ full cells were built by coupling the Li metal anode with a LiFePO$_4$ cathode (8:1:1 of active materials: carbon black: binder). The areal loading of LiFePO$_4$ was about 10 mg cm^{-2}. The cells were tested in a closed system used a LiFePO$_4$ cathode on Al current collector. And porous carbon paper was used as the LiFePO$_4$ cathode current collector in the cells tested in an open O_2 system. Before the O_2 crossover test, the cells were charged to 4.2 V. And then, the cells were cycled in the voltage window of 3.2 to 4.2 V with a limited capacity of 0.2 mA h cm^{-2} at a current density of 0.1 mA cm^{-2}. All cells were assembled in an argon-filled glove box with O_2 and H$_2$O below 0.1 ppm. The EIS test was carried out on a Bio-Logic electrochemical workstation at open circuit potential.

Supporting Information

Supporting Information is available from the Wiley Online Library or from the author.

Conflict of Interest

The authors declare no conflict of interest.

[1] a) C. Zhao, C. Yu, S. Liu, J. Yang, X. Fan, H. Huang, J. Qiu, *Adv. Funct. Mater.* **2015**, *25*, 6913; b) J. Lu, L. Li, J.-B. Park, Y.-K. Sun, F. Wu, K. Amine, *Chem. Rev.* **2014**, *114*, 5611; c) A. C. Luntz, B. D. McCloskey, *Chem. Rev.* **2014**, *114*, 11721; d) P. G. Bruce, S. A. Freunberger, L. J. Hardwick, J.-M. Tarascon, *Nat. Mater.* **2012**, *11*, 19.

**ADVANCED
SCIENCE NEWS**

www.advancedsciencenews.com

**small
methods**

www.small-methods.com

[2] a) S. Wu, J. Yi, K. Zhu, S. Bai, Y. Liu, Y. Qiao, M. Ishida, H. Zhou, *Adv. Energy Mater.* **2017**, *7*, 1601759; b) Y. Liu, P. He, H. Zhou, *Adv. Energy Mater.* **2018**, *8*, 1701602; c) X. B. Zhu, T. S. Zhao, Z. H. Wei, P. Tan, L. An, *Energy Environ. Sci.* **2015**, *8*, 3745; d) X. B. Zhu, T. S. Zhao, Z. H. Wei, P. Tan, G. Zhao, *Energy Environ. Sci.* **2015**, *8*, 2782.

[3] a) X.-B. Cheng, R. Zhang, C.-Z. Zhao, Q. Zhang, *Chem. Rev.* **2017**, *117*, 10403; b) F. Ding, W. Xu, G. L. Graff, J. Zhang, M. L. Sushko, X. Chen, Y. Shao, M. H. Engelhard, Z. Nie, J. Xiao, X. Liu, P. V. Sushko, J. Liu, J.-G. Zhang, *J. Am. Chem. Soc.* **2013**, *135*, 4450; c) M. D. Tikekar, S. Choudhury, Z. Tu, L. A. Archer, *Nat. Energy* **2016**, *1*, 16114; d) D. Lin, Y. Liu, Y. Cui, *Nat. Nanotechnol.* **2017**, *12*, 194.

[4] a) Y. Li, X. Wang, S. Dong, X. Chen, G. Cui, *Adv. Energy Mater.* **2016**, *6*, 1600751; b) J. Yi, S. Guo, P. He, H. Zhou, *Energy Environ. Sci.* **2017**, *10*, 860.

[5] a) Y. Wang, H. Zhou, *Energy Environ. Sci.* **2011**, *4*, 1704; b) T. Zhang, H. Zhou, *Nat. Commun.* **2013**, *4*, 1817; c) N. Bonnet-Mercier, R. A. Wong, M. L. Thomas, A. Dutta, K. Yamanaka, C. Yogi, T. Ohta, H. R. Byon, *Sci. Rep.* **2015**, *4*, 7127; d) G. A. Elia, J. Hassoun, *Sci. Rep.* **2015**, *5*, 12307.

[6] a) X. Wang, D. Zhu, M. Song, S. Cai, L. Zhang, Y. Chen, *ACS Appl. Mater. Interfaces* **2014**, *6*, 11204; b) C. Yu, C. Zhao, S. Liu, X. Fan, J. Yang, M. Zhang, J. Qiu, *Chem. Commun.* **2015**, *51*, 13233; c) H. Kitaura, H. Zhou, *Energy Environ. Sci.* **2012**, *5*, 9077; d) X.-P. Zhang, Z.-Y. Wen, T. Zhang, *J. Mater. Chem. A* **2018**, *6*, 12945; e) X. Zhu, T. Zhao, P. Tan, Z. Wei, M. Wu, *Nano Energy* **2016**, *26*, 565.

[7] H. Kitaura, H. Zhou, *Sci. Rep.* **2015**, *5*, 13271.

[8] a) J. Bae, Y. Li, J. Zhang, X. Zhou, F. Zhao, Y. Shi, J. B. Goodenough, G. Yu, *Angew. Chem., Int. Ed.* **2018**, *57*, 2096; b) M. Balaish, E. Peled, D. Golodnitsky, Y. Ein-Eli, *Angew. Chem., Int. Ed.* **2015**, *54*, 436.

[9] a) X. Cheng, J. Pan, Y. Zhao, M. Liao, H. Peng, *Adv. Energy Mater.* **2018**, *8*, 1702184; b) Z. Tu, Y. Kambe, Y. Lu, L. A. Archer, *Adv. Energy Mater.* **2014**, *4*, 1300654; c) T. Liu, Z. Chang, Y. Yin, K. Chen, Y. Zhang, X. Zhang, *Solid State Ionics* **2018**, *318*, 88.

[10] a) X.-Y. Yang, J.-J. Xu, Z.-W. Chang, D. Bao, Y.-B. Yin, T. Liu, J.-M. Yan, D.-P. Liu, Y. Zhang, X.-B. Zhang, *Adv. Energy Mater.* **2018**, *8*, 1702242; b) Y. Zhang, L. Wang, Z. Guo, Y. Xu, Y. Wang, H. Peng, *Angew. Chem., Int. Ed.* **2016**, *55*, 4487; c) Z. Guo, C. Li, J. Liu, Y. Wang, Y. Xia, *Angew. Chem., Int. Ed.* **2017**, *56*, 7505; d) K.-N. Jung, J.-I. Lee, J.-H. Jung, K.-H. Shin, J.-W. Lee, *Chem. Commun.* **2014**, *50*, 5458; e) J. Zhang, B. Sun, X. Xie, K. Kretschmer, G. Wang, *Electrochim. Acta* **2015**, *183*, 56; f) T. Liu, Q.-C. Liu, J.-J. Xu, X.-B. Zhang, *Small* **2016**, *12*, 3101.

[11] a) W.-B. Luo, S.-L. Chou, J.-Z. Wang, Y.-M. Kang, Y.-C. Zhai, H.-K. Liu, *Chem. Commun.* **2015**, *51*, 8269; b) C. Wu, C. Liao, T. Li, Y. Shi, J. Luo, L. Li, J. Yang, *J. Mater. Chem. A* **2016**, *4*, 15189.

[12] a) C. V. Amanchukwu, H.-H. Chang, M. Gauthier, S. Feng, T. P. Batcho, P. T. Hammond, *Chem. Mater.* **2016**, *28*, 7167; b) L. Wang, Y. Zhang, J. Pan, H. Peng, *J. Mater. Chem. A* **2016**, *4*, 13419.

[13] P. Martins, A. C. Lopes, S. Lanceros-Mendez, *Prog. Polym. Sci.* **2014**, *39*, 683.

[14] J. Luo, C.-C. Fang, N.-L. Wu, *Adv. Energy Mater.* **2018**, *8*, 1701482.

[15] N.-W. Li, Y.-X. Yin, C.-P. Yang, Y.-G. Guo, *Adv. Mater.* **2016**, *28*, 1853.

[16] X.-B. Cheng, T.-Z. Hou, R. Zhang, H.-J. Peng, C.-Z. Zhao, J.-Q. Huang, Q. Zhang, *Adv. Mater.* **2016**, *28*, 2888.

[17] Z. Liang, G. Zheng, C. Liu, N. Liu, W. Li, K. Yan, H. Yao, P.-C. Hsu, S. Chu, Y. Cui, *Nano Lett.* **2015**, *15*, 2910.

[18] G. Zheng, C. Wang, A. Pei, J. Lopez, F. Shi, Z. Chen, A. D. Sendek, H.-W. Lee, Z. Lu, H. Schneider, M. M. Safont-Sempere, S. Chu, Z. Bao, Y. Cui, *ACS Energy Lett.* **2016**, *1*, 1247.

[19] G. Zheng, S. W. Lee, Z. Liang, H.-W. Lee, K. Yan, H. Yao, H. Wang, W. Li, S. Chu, Y. Cui, *Nat. Nanotechnol.* **2014**, *9*, 618.

[20] C. Zhao, C. Yu, M. N. Banis, Q. Sun, M. Zhang, X. Li, Y. Liu, Y. Zhao, H. Huang, S. Li, X. Han, B. Xiao, Z. Song, R. Li, J. Qiu, X. Sun, *Nano Energy* **2017**, *34*, 399.

[21] L. Leng, X. Zeng, P. Chen, T. Shu, H. Song, Z. Fu, H. Wang, S. Liao, *Electrochim. Acta* **2015**, *176*, 1108.